Structure and Dynamics of Graphite Supported Bimetallic Transition Metal Clusters.

Subramanian KRSS, Venkat R. Bhethanabotla[*] and Babu Joseph
Sensors research laboratory, Chemical Engineering Department,
University of South Florida, Tampa, Florida, 33620, USA

Abstract

Supported bimetallic clusters are used extensively in catalysis and sensor applications, with the support used primarily to provide mechanical stability. The properties of metal clusters such as those of gold, platinum, and Cu-Ni on a graphite substrate have been studied in the past and the metal-substrate interactions have been found to result in properties that are different from those of isolated clusters. Understanding of the cluster-substrate interactions at the molecular scale can yield useful insights into parameters that can affect the sensitivity, selectivity and speed of response of sensors, thereby leading to improved designs.

Molecular dynamics simulations have been carried out for Pd-Pt, Pd-Rh and Pd-Cu nanoclusters supported on a static graphite substrate. The Quantum Sutton-Chen potential was utilized for the metal-metal interaction, which we found to be better suited to predict thermal properties of bimetallic system. The graphite substrate is represented as layers of fixed carbons sites, with the Leonard-Jones model potential and parameters utilized in the literature for small molecular physisorption studies. Metal-graphite interaction potentials obtained from fits to experimental cohesive energies were utilized. Monte-Carlo simulations employing the Bond Order simulation model have been used in this work to generate minimum energy initial configurations. These surface segregated initial configurations are utilized as starting configurations in molecular dynamics simulations. Melting characteristics are studied by following the changes in potential energy and heat capacity as functions of temperature. Structural changes accompanying the thermal evolution are studied by the bond order parameter method (BOP). Various thermodynamic, structural and dynamic functions and order parameters are calculated to characterize the structural deformations, melting transitions, wetting characteristics, surface segregation and surface diffusion in these systems. Comparisons with free nanocluster results as well as bulk melting behavior will be presented.

1. Introduction

Metal nanoparticles exhibit physical, chemical and electrical properties that are different from those of bulk materials or single molecules (Edelstein and Cammarata, 1996). These unique properties imparted to nanoparticles by the large fraction of surface atoms, helps them find applications in areas such as heterogeneous catalysis, sensors, as well as micro-electronics. The size, shape and composition of these

[*] Electronic address: venkat@eng.usf.edu

nanoparticles are also known to affect their physical and chemical properties. In sensing applications for instance, the increased surface area leads to improved sensitivity, selectivity and speed of response. One such nanoparticle is Pd which finds extensive use in hydrogen sensing, along with its alloys (Favier, et al., 2001; Chaudhari, 2004). Literature suggests that bimetallics exhibit superior properties in comparison to their single metal counterparts (Sinfelt, 1983). In catalysis and sensing applications, bimetallic nanoparticles supported on substrates such as alumina, graphite, quartz or lithium niobate are commonly used. The behavior of nanoclusters under the influence of a substrate is different from that of isolated nanoclusters (Huang, et al., 2003; Longo, et al., 1999; Antonelli, et al., 1993; Lewis, et al., 2000). The properties in these cases are not only dependent on the particle size and surface composition, but also on the surface morphology and nature of metal-substrate interaction. The key to all potential applications lies in a thorough understanding of thermal, structural and dynamic properties of these nanoparticles especially under the influence of a substrate. Recent advances in experimental techniques (Bardotti, et al., 2000; Prevel, et al., 2004) as well as the insights gained by using first principles calculations such as DFT (Walter, 1999; Zhukovski, et al. 2001; Vervisch, et al., 2002) have led to improved understanding of the same.

During the fabrication process, nanomaterials are subjected to chemical, thermal, and mechanical treatments which alter their surface morphology and hence their catalytic activity. A detailed study of the melting process of metal nanoclusters is critical to understanding their thermal stability (Antonelli, et al., 1993). The melting point is defined as the temperature at which transition from a solid phase with long-range order to a liquid with short-range order occurs. This solid-liquid transition in nanoclusters differs significantly from that in bulk materials (Borel, 1981; Ercolessi and Tosatti, 1991). Both experimental and theoretical studies indicate that melting starts from the surface and propagates to the interior, with the surface melting starting at temperatures significantly lower than the homogeneous transition temperature. (Frenken,1985; Stoltze, 1988; Lewis, 1997). This phenomenon is a result of reduced coordination of surface sites compared to bulk atoms making them less constrained in their thermal motion. Melting at the nanoscale is known to proceed through an intermediate state at which solid and liquid state coexist (dynamic coexistence) and the structure fluctuates between solid and liquid (Cleveland, 1998). Experiments and molecular simulations (Hou, 2000; Bardotti, 2000) give further insights into the dependence of the nanomaterial melting point on their size, shape and composition. In most cases, the cluster melting point is lower than bulk melting values and is known to decrease with cluster size. The variation of melting point is not always monotonic, with quantum effects playing a role at smaller cluster sizes (Garcia-Rodeja, 1994; Calvo, 2000; Lee, 2001).

Previous studies in catalysis and sensing applications have indicated improved selectivity towards specific reactions obtained by controlling surface composition of alloys (Bazin, 1997, 2000). The alloying process leads to variations in shape, structure, and surface atomic distribution depending on nanocluster size, shape, and overall composition. At nanoscale, bimetallic nanoclusters experience a phenomenon known as surface segregation in which one of the metals segregates to the surface. The relative surface energy difference dictates the extent to which segregation occurs (Zhu,

1995). Additional complexities are induced by micromixing. As a result, the melting behavior of alloys differs significantly from that of single component metals.

The presence of substrate induces additional complications. Substrate induced effects on nanoparticle properties are difficult to predict due to the lesser known nature of metal-substrate interactions (Mottet, 2004). Graphite supported cubic and tetrahedral platinum nanocrystals were found to evolve to spherical shapes at temperatures higher than 500 ºC, with surface and total melting occurring at a slightly higher temperature (Wang, 1998). Nanocluster diffusivity on surfaces plays a key role in cluster aggregation processes. Experimental studies suggest rapid diffusion of small antimony clusters on graphite substrates, a fact corroborated by molecular dynamics (MD) studies of Lennard-Jones clusters diffusing on non-epitaxial crystalline surfaces (Bardotti, 1995). Similar MD studies conducted on 249-atom gold nanoclusters indicated high diffusivity of the same on graphite surface (Lewis, 2000). The role played by substrate atoms on the thermal stability and melting behavior of nanoclusters has been studied only to a limited extent. A comprehensive understanding of the structure and dynamics of substrate supported metal nanoclusters and its effect on the melting behavior of bimetallics is needed.

In most of the experimental studies, melting is characterized by changes in shape. This specification is not valid in cases when particles hop from one local minimum to another with increasing temperature (Schmidt, 1997). Thus, shape changes could occur without the particle actually melting. Besides being cost intensive, it is difficult to understand the role played by the substrate through experiments. MD simulations offer a simple and comprehensive tool to understand the complex microscopic phenomena of segregation and micromixing, and insights into the role played by substrate atoms. In the present work, we employ MD simulations to study the dynamics of Pd-Cu, Pd-Rh and Pd-Pt nanoclusters of varying compositions and sizes, supported on a graphite substrate.

2. Initial configuration set-up

All the transition metals under study (Cu, Pd, Pt and Rh) have an FCC structure. Hence, an FCC block/lattice of 500 atoms was constructed from an FCC unit cell by replication in the ABC direction with centre located at (0, 0, 0). The initial atomic positions of the bimetallic system were determined using Metropolis Monte Carlo (MC) simulations employing bond order simulation (BOS) model (Zhu, 1995, 1997). The energy parameters and site energies needed for the BOS model were generated using DFT (Yang, 1994) and the same values have been used in the present study. This approximately cubic nanocluster is supported on a graphite substrate, with the initial metal-substrate distance to 2 Å. The graphite substrate containing 3600 atoms in two layers was built by AB type stacking to have 73.8 x 73.8 x 6.7 Å dimensions. The surface segregation phenomenon present in bimetallic nanoclusters results in lower surface energy atoms being located at low coordination number sites such as surface, edges, and corners. The extent of surface segregation depends on a number of factors such as difference in surface energy, mixing energy, and entropy. The final microstructure is a result of interplay between these factors (Zhu, 1995, 1997). In the present case, the segregation profile of Pd atoms is different amongst the three

bimetallics (Pd-Cu, Pd-Pt and Pd-Rh). In case of Cu-Pd, Cu with much lower surface energy completely segregates to the surface with Pd atoms forming the cluster core. The reverse is true for Pd-Rh where Pd has much lower surface energy than Rh. Pd-Pt represents an intermediate case with more Pd atoms located at the surface than Pt, due to slightly lower surface energy of Pd than Pt.

3. Computational details

3.1 Pair potential function

MD simulations using DL_POLY (Smith, 1999) were performed to gain insights into the melting process at the atomistic level. Each particle is treated as a point mass and is governed by the classical Newton's equations of motion. All the thermodynamic and transport properties were obtained as time averages over the particle positions and velocities. The embedded atom potential (Foiles, 1986) and other long range potentials like the Sutton-Chen potential (Sutton and Chen , 1990) based on Finnis-Sinclair type of potentials have been used in the literature successfully to predict the properties of FCC based metals such as Pd, Cu, Rh and Pt. The local electronic density is included to account for the many body terms.

Based on the Sutton-Chen potential, the potential energy of the finite system is given by,

$$U_{tot} = \sum_i U_i = \sum_i \varepsilon \left[\sum_{j \neq i} \frac{1}{2} V(r_{ij}) - c\rho_i^{1/2} \right] \tag{3.1}$$

Here, V (r_{ij}) is a pair potential to account for the repulsion resulting from Pauli's exclusion principle.

$$V(r_{ij}) = \left(\frac{a}{r_{ij}} \right)^n \tag{3.2}$$

The local density accounting for cohesion associated with any atom i is given by,

$$\rho_i = \sum_{j \neq i} \phi(r_{ij}) = \sum_{j \neq i} \left(\frac{a}{r_{ij}} \right)^m \tag{3.3}$$

Sutton and Chen restricted values of m to be greater than 6 and fitted it to give close agreements with bulk modulus and the elastic constants. The Sutton-Chen potential predicts properties involving defects, surfaces and interfaces poorly. The Quantum Sutton-Chen (Cagin, 1990) (hereafter referred to as QSC), which is a modification of the Sutton-Chen potential, includes quantum corrections and takes into account the zero point energy allowing better prediction of temperature dependent properties. The QSC potential function was found to be better suited to melting and phase transformation studies of bulk Cu-Ni and Cu-Au alloys (Qi, 1999, 2002). The QSC parameters for the metal atoms are listed in Table 1. The geometric mean was

used to obtain the energy parameter ε and the arithmetic mean was used for the remaining parameters, to predict the nature of interaction between metal atoms.

Our studies indicate that the QSC potential functions predict the thermal properties of transition metal alloys better than SC potentials (Subramanian, 2004). Therefore, we have used QSC potential function in all our nanocluster studies presented here. To represent the relatively weak interactions between the carbon atoms in the graphite substrate and an adsorbed metal atom, the LJ potential function has been used. Previous work on substrate supported clusters indicates that the LJ potential for this interaction provides reasonable predictions of the complex system (Huang, 2003). Hence, we employ LJ (12-6) model for metal-C interactions. The LJ parameters (ε=0.002413 eV, σ = 3.4 A) for graphite have already been determined (Bhethanabotla, 1990). The LJ parameters for metal atoms were taken from published values and Lorentz-Berthelot mixing rules were employed to find well depth and size parameters for metal-C interactions. A static substrate with fixed positions of C atoms was used to reduce the computational load.

3.2 MD simulation details

The MD simulations were carried out in an ensemble approximating the canonical with a constant number of atoms N and volume V (much larger than the cluster size) without any periodic boundary conditions. A constant temperature Berendson thermostat with a relaxation time of 0.4 ps was used. The equations of motion were integrated using Verlet leapfrog algorithm with a time step of 0.001 ps. The nanocluster was initially subjected to mild annealing in the 0-300 K interval. This was followed by heating to 1800 K in increments of 100 K. Near the melting point, the temperature increments were reduced to 10 K to account for the large temperature fluctuations. The simulations were carried out for 400 ps of equilibration followed by production time of 200 ps for generating time averaged properties.

Table 1. Potential parameters used in MD simulations for metal-metal interactions

Quantum Sutton-Chen	n	m	ε (eV)	C	a(Å)
Pd	12	6	3.2864e-3	148.205	3.8813
Pt	11	7	9.7894e-3	71.336	3.9163
Rh	13	5	2.4612e-3	305.499	3.7981
Cu	10	5	5.7921e-3	84.843	3.603

4. Results and discussion

4.1 Melting point identification

The transition temperature from solid to liquid phase is usually identified by studying the variation in either the thermodynamic properties such as potential energy and specific heat capacity or some structural properties such as Bond Order Parameters and Wigner values. The present study employs both these methods to identify melting points for different cluster sizes and compositions. Details are discussed in subsequent sections.

4.2.1 Potential energy

Figure 1 shows the temperature dependence of potential energy for the $(Pd_{0.5}\text{-}X_{0.5})_{500}$ atom clusters where X=Pt, Rh or Cu. The transition from a solid to a liquid phase can be identified by a simple jump in the total potential energy curve. This corresponds to a melting temperature of 1390 ±10K for $(Pd_{0.5}\text{-}Pt_{0.5})_{500,}$ 1540 K ±10K for $(Pd_{0.5}\text{-}Rh_{0.5})_{500}$ and 1020 ±10K for $(Pd_{0.5}\text{-}Cu_{0.5})_{500}$, as seen in Figure 1. The variation of potential energy with temperature for clusters of different compositions is discussed in subsequent sections. These melting temperatures are at least 100-200 K higher than that for isolated clusters of similar composition and size. The delay in the onset of the melting point could be a result of the lesser degree of freedom of atoms close to the substrate. The implications of the graphite support on the dynamics of cluster melting will be discussed in subsequent sections.

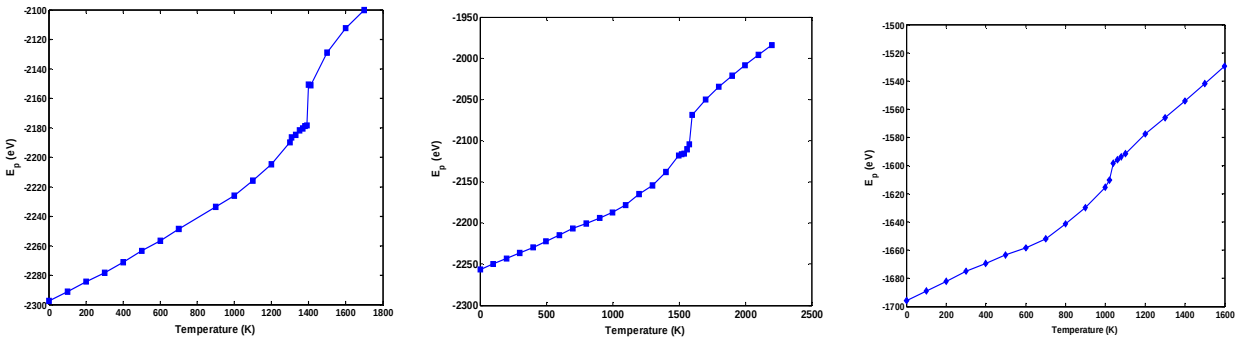

(a) **(b)** **(c)**

Figure 1. Potential energy variation with temperature for $(Pd_{0.5}\text{-}X_{0.5})_{500}$ clusters (a) X=Pt (b) X=Rh (c) X=Cu

4.2.2 Specific heat capacity

The specific heat capacity in a weak coupling ensemble such as achieved with the Berendson thermostat can be written as a function of fluctuations in the potential energy $<(\delta E_p)^2>$ (Morishita, 2000).

$$C_v = \frac{k < (\delta E_p)^2 >}{(kT)^2 - 2\alpha < (\delta E_p)^2 > / 3N} \qquad (4.1)$$

where $< (\delta E_p)^2 > = < E_p^2 > - < E_p >^2$ and α is the ratio of the standard deviations of kinetic and potential energies.

$$\alpha = \sqrt{< (\delta KE)^2 > / < (\delta Ep)^2 >} \qquad (4.2)$$

Morishita has proved that a weak coupling ensemble approaches a canonical ensemble for very short relaxation times (α ≈ 0) and to a microcanonical ensemble for longer relaxation times (α ≈ 1). In the present case, the Berendson thermostat with a coupling parameter of 0.4 ps leads to α ≈10^{-4}, making the calculations for specific heat capacity similar to that of a canonical ensemble as given in equation (4.3)

$$C_v = \frac{k\left\langle (\delta E_p)^2 \right\rangle}{(kT)^2} \qquad (4.3)$$

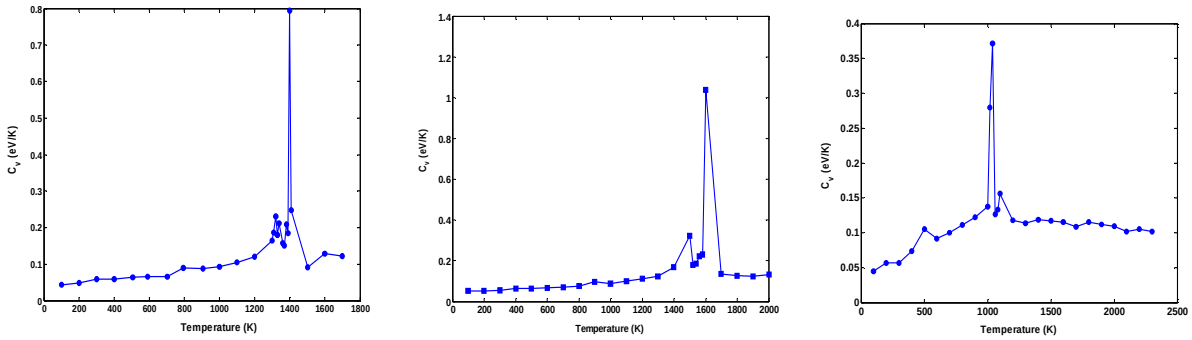

(a) **(b)** **(c)**

Figure 2. Variation of specific heat capacity with temperature for $(Pd_{0.5}\text{-}X_{0.5})_{500}$ clusters (a) X=Pt (b) X=Rh (c) X=Cu

To identify the melting temperature, the specific heat capacity at constant volume is plotted in Figure 2. For all three $(Pd_{0.5}\text{-}X_{0.5})_{500}$ clusters, the maximum in the specific heat capacity corresponds to the temperature where a jump in potential energy is observed i.e 1390 ±10K for X=Pt, 1540 K ±10K for X=Rh and 1020 ±10K for X=Cu. This leads to a melting temperature estimates of T_m=1390 ± 10 K, 1540 K ±10K, and 1020 ±10K for $(Pd_{0.5}\text{-}Pt_{0.5})_{500}$, $(Pd_{0.5}\text{-}Rh_{0.5})_{500}$, and $(Pd_{0.5}\text{-}Cu_{0.5})_{500}$, respectively. The small peaks in the specific heat capacity curve at temperatures lower than the actual melting point indicate onset of surface melting. The more prominent peak in case of Pd-Cu would mean that the extent of surface melting is much more than in Pd-Pt and Pd-Rh. Indeed, experiments suggest Pd and Cu to surface melt a lot more than Pt and Rh.

4.2.3 Bond order parameter

There are several criteria used to identify local and extended orientational symmetries. One such method is the Bond Order Parameter method (Steinhardt, 1983), which is used to analyze cluster structure as well as to distinguish between atoms in solid (closed packed) and liquid environment generated at the onset of melting. To determine the orientational order, spherical harmonic basis functions $Y_{lm}(\theta_{ij},\varphi_{ij})$ are associated with every bond joining an atom to its near neighbors. Here, Θ and Φ refer to polar and azimuthal angles of vector $\boldsymbol{r}_{ij}$ in a given reference frame. The term "bond" refers to the unit vector $\boldsymbol{r}_{ij}$ joining a reference atom *i* to any neighboring atom *j* within a cutoff radius r_{cut}. The cutoff radius is generally taken to be 1.2 times the first minimum in the radial distribution function. The function is calculated as an average over all atoms, surface and interior, and ensures all atoms in the first coordination shells are counted as near neighbors. To make the bonds independent of direction, only even *l* shaped harmonics are considered which are invariant under inversion. The local order around any atom *i* is an average over all its bonds with the neighboring N_{nb} atoms and given by

$$q_{lm}(i) = \frac{1}{N_{nb}(i)} \sum_{j=1}^{N_{nb}(i)} Y_{lm}(r_{ij}) \tag{4.4}$$

A second order invariant can be constructed to give a local order parameter independent of the choice of reference system.

$$q_l(i) = \left(\frac{4\pi}{2l+1} \sum_{m=-l}^{l} | q_{lm}(i) |^2 \right)^{1/2} \tag{4.5}$$

An average of q_{lm} over all N atoms in a cluster gives the global bond order parameter.

$$Q_l = \left(\frac{4\pi}{2l+1} \sum_{m=-l}^{l} \left| \overline{Q}_{lm} \right|^2 \right)^{1/2} \tag{4.6}$$

where,

$$\overline{Q}_{lm} = \frac{\sum_{i=1}^{N} N_{nb} q_{lm}(i)}{\sum_{i=1}^{N} N_{nb}(i)} \tag{4.7}$$

The value of the global bond order parameter Q_l in a solid cluster depends on the relative bond orientations and has a unique value for each crystal structure. Based on local solid symmetry, it was found that cubic and decahedral clusters have nonzero values of $q_l(i)$ for $l \geq 4$ and at $l = 6$ for those with icosahedral symmetry. All global order parameters vanish in isotropic liquids for $l > 0$. The global bond order values for different types of symmetry are reported in

Table 2. The atoms in a solid undergo vibrations about their equilibrium positions leading to distortion of the crystal structure which is characterized by Q_4 and Q_6 values. The magnitude of the nonzero $\{Q_l\}$ values depends on the definition of nearest neighbors and can be changed by including surface bonds in the average. The cutoff distance (r_{cut}) for identifying the nearest neighbors was taken to be 3.6 A at 300 K. This corresponds to the position of the first minimum in the pair correlation function for FCC Pd-Pt. Similarly, r_{cut} at other temperatures were identified.

Table 2. Bond Order Parameter values for various geometries.

Geometry	Q_4	Q_6
FCC	0.19094	0.57452
HCP	0.09722	0.48476
BCC	0.03637	0.51069
Icosahedral	0	0.66332
Sc	0.76376	0.35355
Liquid	0	0

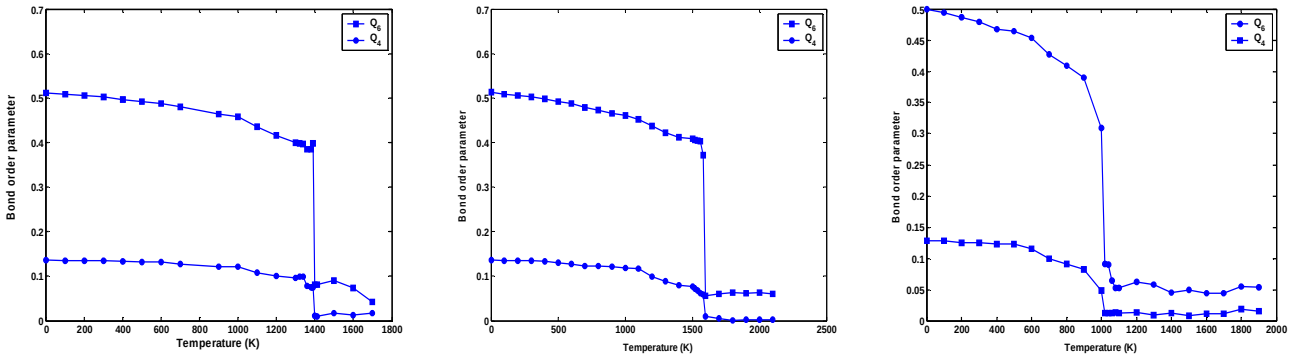

(a) **(b)** **(c)**

Figure 3. Variation of bond order parameters with temperature for $(Pd_{0.5}\text{-}X_{0.5})_{500}$ clusters (a) X=Pt (b) X=Rh (c) X=Cu

Figure 3 indicates the variation in bond order parameter with temperature for the three bimetallics. All the three bimetallics show rapid structural rearrangement when subjected to annealing between 0-300K. The change in order parameters of Pd-Cu is much steeper than in the cases of Pd-Rh and Pd-Pt. The rapid structural changes in the Pd-Cu might be attributed to the early onset of surface melting. The effect of substrate on the surface melting characteristics of the clusters needs to be explored further. At the melting point, the order parameters of all the three nanoclusters show a sudden decrease to zero indicating the transition from solid to liquid phase. The melting points found using these order parameters matches those found using potential energy and specific heat capacity curves.

5. Conclusions

The melting characteristics of graphite supported bimetallic clusters have been studied using MD simulations. The melting points of bimetallic nanoclusters have been found by studying variations of thermodynamic and structural properties with temperature. In all the cases, the effect of support is to delay the onset of melting leading to higher transition temperatures compared with isolated nanoclusters, but still lower than bulk melting points. Specific melting temperature depends on nanocluster size and composition. Our studies indicate that structural solid-solid transitions take place at temperature much below the phase transition. The extent of surface melting in the three cases seem to be widely different and the role played by the substrate needs to be investigated further.

The dynamics of substrate supported cluster melting are being studied using deformation parameters, diffusion coefficients, and analysis of density profiles. The effect of cluster composition on melting of graphite supported nanoclusters would also be studied. Our preliminary results indicate a non-linear variation of melting points with composition. The role of the support in this variation needs to be investigated further. We find the cluster to diffuse as a single entity on the graphite surface. Quantification of the same needs to be done by studying the variation of cluster diffusion coefficients with temperature. Previous studies indicate that wetting behavior is influenced by the nature of the metal-metal interactions. In the present case, the impact of metal-graphite interactions on the wetting characteristics of the liquid nanocluster needs to be investigated. A melting theory for substrate supported nanoclusters would provide better insights into the melting phenomenon.

References

1. Agrawal, P. M.; Rice, B. M.; Thompson, D. L. Predicting trends in rate parameters for self-diffusion on FCC metal surfaces. Surf. Sci. 2002, 515(1): 21-35.
2. Allen, M. P and Tildesley, D. J: Computer Simulation of Liquids. 1987, Oxford University Press.
3. Antonelli, A.; Khanna, S. N.; Jena, P. Thermal stability of supported metal clusters. Phys. Rev. B: Condensed Matter and Materials Physics 1993, 48(11), 8263-6.
4. Bardotti, L.; Prevel, B.; Melinon, P. et al. Deposition of Au-N clusters on Au(111) surfaces. II. Experimental results and comparison with simulations. Phys. Rev. B 2000, 62 (4): 2835-2842.
5. Bardotti, P. L.; Jensen, A. H.; Treilleux, M. and Cabaud, B. Experimental Observation of Fast Diffusion of Large Antimony Clusters on Graphite Surfaces, Phys. Rev. Lett. 1995, 74: 4694.
6. Bazin, D.; Kovacs, I.; Lynch, J. et al. Ru-Co/NaY bimetallic catalysts: in situ EXAFS study at CoK- and RuK-absorption edges. Appl. Catalysis A-General 2003, 242 (1): 179-186.
7. Bazin, D.; Mottet, C.; Treglia, G. New opportunities to understand heterogeneous catalysis processes on nanoscale bimetallic particles through synchrotron radiation and theoretical studies. Appl. Catalysis A-General 2000, 200 (1-2): 47-54.
8. Bazin, D.; Sayers, D.; Rehr J. J. et al. Numerical simulation of the platinum L-III edge white line relative to nanometer scale clusters. J. Phys. Chem. B 1997, 101 (27): 5332-5336.
9. Bhethanabotla, V. R, Steele, W. A. Computer-simulation study of melting in dense oxygen layers on graphite. Phys. Rev. B 1990, 41 (13): 9480-9487.
10. Borel, J. P. Thermodynamical size effect and the structure of metallic clusters Surf. Sci. 1981, 106 (1-3): 1-9.
11. Cagin, T.; Kimura, Y.; Qi, Y.; Li, H.; Ikeda, H.; Johnson, W.L.; Goddard, W.A. III. Mater. Res. Soc. Symp. Proc. 1999, 554(Bulk Metallic Glasses): 43-48.
12. Calvo, F.; Spiegelmann, F. Mechanisms of phase transitions in sodium clusters: from molecular to bulk behavior. J. Chem. Phys. 2000, 112(6): 2888-2908.
13. Chaudhari, A. Master's Thesis (USF), 2004.
14. Cleveland, C. L.; Luedtke, W. D.; Landman, U. Melting of Gold Clusters: Icosahedral Precursors. Phys. Rev. Lett. 1998, 81(10): 2036-2039.
15. Edelstein, A.S; Cammarata, R.C. (Ed.) Nanomaterials: Synthesis, Properties and Applications.1996, Institute of Physics Publishing, Bristol and Philadelphia
16. Ercolessi, F.; Andreoni W.; Tosatti, E. Melting of small gold particles – Mechanism and size effects. Phys. Rev. Lett. 1991, 66 (7): 911-914.
17. Favier, F.; Walter, E. C.; Zach, M. P. et al. Hydrogen sensors and switches from electrodeposited palladium mesowire arrays. Science 2001, 293 (5538): 2227-2231.
18. Foiles, S.M.; Baskes, M.I., and Daw, M.S. Embedded-atom-method functions for the fcc metals Cu, Ag, Au, Ni, Pd, Pt, and their alloys. Phys. Rev. B 1986, 33 (12): 7983-91.

19. Frenken, J. W. M.; Van der Veen, J. F. Observation of Surface melting. Phys. Rev. Lett. 1985, 54(2), 134-137.
20. Garcia-Rodeja, J.; Rey, C.; Gallego L. J. et al. Molecular-Dynamics study of the structures, binding-energies, and melting of clusters of FCC transition and noble metals using the Voter and Chen version of the embedded atom model. Phys. Rev. B 1994, 49 (12): 8495-8498.
21. Hou, Q.; Hou, M.; Bardotti, L. et al. Deposition of Au-N clusters on Au(111) surfaces. I. Atomic-scale modeling. Phys. Rev. B 2000, 62 (4): 2825-2834.
22. Huang, S-P. and Balbuena, P. B. Platinum nanoclusters on graphite substrates: a molecular dynamics study. Mol. Phys. 2002, 100(13), 2165-2174.
23. Huang, S-P; Mainardi, D. S.; Balbuena, P. B. Structure and dynamics of graphite-supported bimetallic nanoclusters. Surf. Sci. 2003, 545(3), 163-179.
24. Lee, Y. J.; Lee, E. K.; Kim, S.; Nieminen, R. M. Effect of potential energy distribution on the melting of clusters. Phys. Rev. Lett. 2001, 86(6): 999-1002.
25. Lewis, L. J.; Jensen, P.; Barrat, J-L. Melting, freezing, and coalescence of gold nanoclusters. Phys. Rev. B: Condensed Matter 1997, 56(4): 2248-2257.
26. Lewis, L. J.; Jensen, P.; Nicolas, C.; Barrat, J-L. Diffusion of gold nanoclusters on graphite. Phys. Rev. B: Condensed Matter and Materials Physics 2000, 61(23): 16084-16090.
27. Longo, R. C.; Rey, C.; Gallego, L. J. Structure and melting of small Ni clusters on Ni surfaces. Surf. Sci. 1999, 424(2-3): 311-321.
28. Morishita, T. Fluctuation formulas in molecular-dynamics simulations with the weak coupling heat bath. J. Chem. Phys. 2000, 113(8): 2976-2982.
29. Mottet, C.; Goniakowski, J.; Baletto, F.; Ferrando, R.; Treglia, G. Modeling free and supported metallic nanoclusters: structure and dynamics. Phase Transitions. 2004, 77(1-2): 101-113.
30. Prevel, B.; Bardotti, L.; Fanget, S.; et al. Gold nanoparticle arrays on graphite surfaces. Appl. Surf. Sci. 2004, 226 (1-3): 173-177.
31. Qi, Y.; Cagin, T.; Kimura, Y., et al. Viscosities of liquid metal alloys from non-equilibrium molecular dynamics. J. Comp-Aided Mat. Des 2002, 8 (2-3): 233-243.
32. Qi Y, Cagin T, Kimura Y, et al. Molecular-dynamics simulations of glass formation and crystallization in binary liquid metals: Cu-Ag and Cu-Ni. Phys. Rev. B 1999, 59 (5): 3527-3533.
33. Schmidt, M.; Kusche, R.; Kronmuller, W.; von Issendorff, B.; Haberland, H. Experimental determination of the melting point and heat capacity for a free cluster of 139 sodium atoms. Phys. Rev. Lett. 1997, 79(1): 99-102.
34. Sinfelt, J. H. Bimetallic Catalysts-Discoveries, Concepts, and Applications. 1983 John Wiley & Sons: New York.
35. Smith, W. and Forester T. R. DL_POLY 1996, Daresbury Laboratory, Daresbury.
36. Steinhardt, P. J.; Nelson, D. R.; Ronchetti, M. Bond-orientational order in liquids and glasses. Phys. Rev. B: Condensed Matter and Materials Physics 1983, 28(2): 784-805.
37. Stoltze, P.; Norskov J. K.; and Landman, U. Phys. Rev. Lett. Disordering and melting of aluminum surfaces. 1988, 61, 440.
38. Subramanian, K. R. S. S.; Bhethanabotla, V. R.; Joseph, B. A Molecular Dynamics Simulation Study on Melting of Pd-Pt Nanoclusters, Unpublished work.

39. Sutton, A. P and Chen, J. Philos. Mag. Lett. Long range Finnis-Sinclair potentials. 1990, 61: 139-146.
40. Vervisch, W, Mottet, C. and Goniakowski, J. Theoretical study of the atomic structure of Pd nanoclusters deposited on a MgO(100) surface. Phys. Rev. B 2002, 65: 245411
41. Walter, E. (Ed.) Metal Clusters. 1999, Wiley series in theoretical chemistry.
42. Wang, Z. L.; Petroski, J. M.; Green, T. C.; El-Sayed, M. A. Shape Transformation and Surface Melting of Cubic and Tetrahedral Platinum Nanocrystals. J. Phys. Chem. B 1998, 102(32): 6145-6151.
43. Yang, L. and DePristo, A. E. On the compact structure of small fcc metal clusters. J. Catalysis 1994, 149(1): 223-8.
44. Zhu, L. and DePristo, A. E. Bond order simulation model: coordination dependent bimetallic bonds. J. Chem. Phys. 1995, 102(13): 5342-9.
45. Zhu, L. and DePristo, A. E. Microstructures of bimetallic clusters: bond order metal simulator for disordered alloys. J. Catalysis 1997, 167(2): 400-407.
46. Zhukovskii, Y. F., Kotomin, E.A., Fuks, D., Dorfman, S., et al. Hartree-fock study of adhesion and charge redistribution on the Ag/MgO (001) interface. Surf. Sci. 2001, 482: 66